Contents lists available at SciVerse ScienceDirect

Applied Catalysis B: Environmental

Selection of oxygen reduction catalysts for rechargeable lithium–air batteries—Metal or oxide?

H. Cheng*, K. Scott

School of Chemical Engineering & Advanced Materials, Newcastle University, NE1 7RU, UK

ARTICLE INFO

ABSTRACT

Carbon-supported Pd and PdO nanocatalysts were synthesised using either chemical reduction or thermal synthesis procedures and were used as model metal and oxide catalysts for oxygen reduction in rechargeable lithium–air batteries. The Pd metal catalyst showed excellent initial performance, e.g. a discharge capacity of 855 mAh (g solids)$^{-1}$. However, the PdO catalyst displayed superior capacity retention to the Pd catalyst, producing a discharge capacity of 336 mAh (g solids)$^{-1}$ after 10 cycles, i.e. the capacity retention was 6% per cycle. The activity and stability of Pd metal and oxide catalysts were found to be closely related to their intrinsic catalytic properties and structural changes during charge/discharge cycles in Li–air batteries. The implication of such a difference is discussed. Model Pd/C and PdO/C catalysts were compared with other widely used carbon-supported metal and oxide catalysts, including Pt/C, Ru/C, RuO$_2$/C and MnO$_2$/C.

1. Introduction

To meet the demand for higher power and better energy storage capabilities, much attention has been focused on the development of rechargeable Li batteries [1–5]. A revolutionary advance from graphite–LiCoO$_2$ batteries to Li–air counterparts has recently emerged. These latter batteries allow lithium ions to react with oxygen from atmospheric air, external to the battery as needed. In terms of specific capacity, lithium metal–air batteries are able to deliver up to 5.2×10^3 Wh kg^{-1} including the weight of oxygen, which is ten-times that of current high-performance lithium-ion batteries and more than any other class of energy-storage device [1–5]. In addition, lithium–air batteries are compact, lightweight and cost-effective because they adopt cheap and light materials that use oxygen drawn from the air during discharge, replacing expensive chemical constituents used in current rechargeable batteries. Apparently, it could make batteries more complex and lead to the loss of compactness if usual desiccate and units were adopted to remove CO$_2$ or other harmful gases. However, it could be possible to remove CO$_2$ or other harmful gases from batteries using novel technologies, such as membrane separation technology, rather than complex desiccate and units, which should greatly increase volume and weight of batteries. Therefore, the lithium–air battery could be a small and light weight battery, suitable for hybrid electric vehicles. It also has the potential to give a major boost to the renewable energy industry, as the battery will provide back up power to enable a constant electrical output from intermittent renewable sources such as wind or solar.

Early investigation of Li–air batteries showed that the air cathode was the most important challenge for their development [1,2]. Nano-materials are of interest because of their relatively large surface area, which enables faster reaction rates, and their short diffusion path lengths compared to the bulk. Moreover, it is well known that materials structured at the nanoscale have different thermodynamic, electronic and mechanical properties than in the bulk form and this provides a great opportunity for the development of novel energy-storage devices [6,7]. A typical example was nano-structured manganese oxides [8–10]. Particularly, MnO$_2$ is of great interest for lithium batteries due to its low cost, lower toxicity and higher average voltage and its energetic compatibility in a reversible lithium electrochemical system, compared to vanadium-based oxides [11]. Composite electrode materials, such as amorphous manganese oxide coated onto acetylene black, have demonstrated relatively high discharge-specific capacity [12]. However, there remains the challenge of achieving practical recharge ability for its use as the positive electrode in lithium secondary batteries and better positive electrode materials for lithium–air batteries are required. The performance of MnO$_2$ cathodes in the Li–air batteries and their Li-ion counterparts is not totally comparable because they are different types of batteries, although MnO$_2$ cathodes in these batteries have some similar role. Recently, a rechargeable oxygen electrode for lithium batteries was

* Corresponding author. Fax: +44 0191 222 5292.
E-mail address: hua.cheng@ncl.ac.uk (H. Cheng).

made by mixing Super S carbon powder, electrolytic manganese dioxide catalysts and Kynar 2801 polymer binder to form a porous composite material [3,4]. In situ mass spectrometry measurements confirmed that oxygen reduction was reversible on such an oxygen electrode, i.e. the Li_2O_2 formed on discharging the oxygen electrode was decomposed to Li and O_2 during charging. Charge/discharge cycling on such an oxygen electrode was also sustainable [4].

Very recently, carbon-supported platinum and gold catalysts have been found to affect the charge and discharge voltages of rechargeable lithium–oxygen batteries and thus enable higher efficiency than simple carbon electrodes in such batteries [13]. However, both platinum and gold are expensive. Moreover, data were collected in a short period. This means that the work did not address the cycle life of such devices, thus leaving open question of suitability of the catalysts.

Our recent work demonstrated that discharge capacities could be improved by using carbon-supported manganese oxide as oxygen reduction catalysts, providing a material specific energy of 4750 mAh (g carbon)$^{-1}$ upon cycling to 4.3 V [14]. This increase in energy storage could be related to uniformly distributed catalysts in the carbon matrix, leading to an enhanced activity for oxygen reduction and an improved electrical connection among the catalyst and current collectors. Moreover, the cycling stability of this material was relatively high, which could be in part attributed to its intrinsic structural stability against severe reduction conditions [14]. The work also showed the importance of optimising oxygen electrodes for the development of practical rechargeable lithium–air batteries [14].
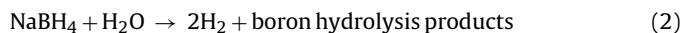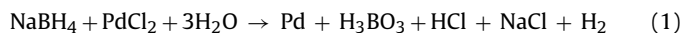
As mentioned above, both metal and oxide catalysts were used in rechargeable Li–air batteries [4,13,14]. Our investigation showed that metal and oxide catalysts had significant differences in activity for oxygen reduction and stability during charge/discharge cycles in rechargeable Li–air batteries. Thus in this study we choose carbon-supported Pd and PdO nanocatalysts as model metal and oxide systems. This selection is based on the following facts: (i) Pd and Pd alloy catalysts have been used increasingly for oxygen electroreduction due to their advantages, such as lower cost and comparable activity for oxygen reduction reaction, compared with Pt catalysts [15–20]. (ii) Activity of PdO catalysts for oxygen reduction in aqueous solutions was demonstrated previously and, instead of a single four-electron transfer, oxygen reduction at PdO electrodes partially proceeded via a pair of two-electron transfers [21]. Even for Pd and Pd-containing electrodes, palladium oxide species were actively involved in processes of oxygen reduction and PdO showed higher stability than Pd under oxygen reduction conditions [22,23]. With the aid of Pd/C and PdO/C as model oxygen reduction catalysts in rechargeable lithium–air batteries, we attempt to understand the difference of metal and oxide catalysts and, possibly, provide some clues to guide the choice of cathode catalysts for rechargeable Li–air batteries. To reach this end, apart from using severe charge/discharge cycling test, scanning electron microscopy (SEM), energy dispersive X-ray spectroscopy (EDX), transmission electron microscopy (TEM) and X-ray diffraction (XRD) and impedance techniques were used to provide insight of the involvement of Pd/C and PdO/C model catalysts in the oxygen reduction reaction. Model Pd/C and PdO/C catalysts were also compared with other carbon-supported metal and oxide catalysts that were widely used as catalysts for oxygen reduction in both aqueous solutions and in non-aqueous media, including Pt/C, Ru/C, RuO_2/C and MnO_x/C.

2. Experimental

2.1. Catalyst fabrication

Carbon-supported Pd, Pt and Ru catalysts were prepared by chemical reduction methodology, modified from the literature [24].

For example, Pd/C catalysts were obtained by chemical reduction of $PdCl_2$ using $NaBH_4$:

$$NaBH_4 + PdCl_2 + 3H_2O \rightarrow Pd + H_3BO_3 + HCl + NaCl + H_2 \quad (1)$$

$$NaBH_4 + H_2O \rightarrow 2H_2 + \text{boron hydrolysis products} \quad (2)$$

In practice, under ultrasonic agitation, 200 mg Norit carbon black powder (SX, Norit) in 200 cm^3 (ml) deionised water were heated in a water jacketed closed glass container to 60 °C, using a thermal circulating water bath (TE-10A, Techne), for 30 min. Then, a dilute aqueous HCl solution containing 220 mg $PdCl_2$ (99%, Aldrich) were added into the mixture. The $PdCl_2$ catalysts were then reduced by adding excess 0.2 mol dm^{-3} (M) $NaBH_4$ solutions, drop by drop, until the water turned black. Once the Pd black was then filtered from the mixture and washed with deionised water. The produced materials were dried in the oven under nitrogen atmosphere at 105 °C for 2 h. The resulting Pd/C catalyst had a metal loading of ca. 40%, as estimated from the EDX measurement. The Pt/C and Ru/C catalysts had a similar metal loading of approximately 40%. Therefore, they had a metal catalyst/carbon ratio of 40:60 in weight (Table 1).

Carbon-supported PdO and RuO_2 catalysts were prepared by a modified procedure based on previous reports [25–27] using $PdCl_2$ ($\geq$99.9%, Aldrich) and $RuCl_3$ (Ru content 45–55%, Aldrich) as precursors. In brief, starting Norit carbon black powder was impregnated with $PdCl_2$ and $RuCl_3$ solutions and the chlorides were thermally oxidised at high temperature (500–550 °C) under air atmosphere:

$$Pd^{2+} \frac{1}{2}O_2 \rightarrow PdO \quad (3)$$

$$Ru^{3+} + O_2(\text{heat}) \rightarrow RuO_2 \quad (4)$$

The selection of conditions for catalyst treatment was considering that carbon materials could be purified and their electrochemical properties could be improved by oxidising in air up to 550 °C with little loss in weight [28–32].

For example, carbon-supported PdO catalysts were produced by adding 50 ml aqueous solution containing 1 g $PdCl_2$, drop by drop, to a suspension of 0.95 g Norit carbon black powder in 150 ml water at 60 °C under vigorous ultrasonic agitation. The solvent was filtered and the residue was washed with water. The dried powder was exposed to 100 ml min^{-1} air flow at 550 °C for 4 h. The resulting PdO/C catalyst had an oxide loading of ca. 40 wt%. The RuO_2/C also had an oxide loading of approximately 40 wt%. This means that the ratio of oxide catalyst/carbon were 40:60 in weight (Table 1).

Details of synthesis of carbon-supported manganese oxides (MnO_2/C) were described elsewhere [14]. In brief, it was based on a redox reaction of manganese sulphate and potassium permanganate in the presence of a carbon matrix:

$$2MnO_4^- + 3Mn^{2+} + 2H_2O \rightarrow 5MnO_2 + 4H^+ \quad (5)$$

In practice, a closed glass container with a water jacket containing 150 ml water were heated to 80 °C using a thermal circulating water bath (TE-10A, Techne). Under magnetic stirring, 1.0 g carbon powder were added to the hot water and stirred for 20 min at 80 °C. Then 0.4 g $MnSO_4 \cdot H_2O$ (99%, Sigma) and 1.1 g $KMnO_4$ (99.5%, BDH) were dissolved in 25 ml hot water (80 °C) separately. Both solutions were added to the container, drop by drop, under magnetic stirring and kept at 80 °C for 1 h. The suspension was filtered and washed several times using distilled water, and then dried at 120 °C overnight. The produced materials were treated at several temperatures but only results obtained using the best catalyst (annealed at 300 °C) sample are reported in this paper. The material had a catalyst loading of around 27 wt% for Mn and 43 wt% for MnO_2. The valence number of the MnO_x oxide used in this study was approximately 2, as estimated from the EDX measurement (Table 1), which produced the best activity among our tested manganese oxides.

Table 1
Compositions of carbon-supported catalysts.[*]

Catalyst	Composition (wt%)						Composition (at.%)					
	C	Pd	Pt	Ru	Mn	O	C	Pd	Pt	Ru	Mn	O
Pd/C	59.97	40.03					92.99	7.01				
Pt/C	59.88		40.12				96.04		3.96			
Ru/C	59.85			40.15			92.62			7.38		
PdO/C	58.48	36.79				4.73	88.36	6.27				5.37
RuO$_{2.0}$	58.21			31.74		10.05	83.72			5.43		10.85
MnO$_{2.0}$	57.24				27.02	15.74	76.36				7.88	15.76

[*] Measured by the EDX technique.

To make meaningful comparison, the catalyst loading in all cathode composites was kept at 1 mg metal cm^{-2}.

2.2. Material characterisation

Scanning electron microscope and energy-dispersive X-ray analyses were carried out using a JEOL JSM-5300LV scanning electron microscope at an acceleration voltage of 25 kV, combined with a ROUTEC UHV Dewar Detector.

Transmission electron microscopy images were taken using a Philips CM100 transmission electron microscope. The TEM sample preparation included embedding and sectioning steps. In the embedding step, the composite electrode material was embedded in 100% resin (Epoxy embedding resin kit (medium), TAAB Lab. Equip., Aldermaston, Berks) at 60 °C for 24 h. Then ultrathin sections (80 nm approximately) were cut from the composite electrode material using a diamond knife (Diatome 35°) on a RMC MT-XL ultramicrotome. The sections were stretched with chloroform to eliminate compression and, finally, mounted on Pioloform filmed copper TEM grids (Agar Scientific, Stansted, Essex). The grids were examined using a Philips CM 100 Compustage (FEI) Transmission electron microscope and digital images collected using an AMT CCD camera (Deben).

X-ray diffraction analysis was performed using a Cu Kα radiation with a Siemens D-5005 X-ray Diffractometer at a tube current of 100 mA and a tube voltage of 40 kV. The 2θ angular regions between 20° and 100° were explored at a scan rate of 2° min^{-1}. The XRD patterns were compared to the International Centre for Diffraction Data® (ICDD®) [33].)

2.3. Impedance analysis

The electrochemical impedance spectra were measured in situ of batteries where the cathode was fed with oxygen or argon. The anode served as both reference electrode and counter electrode. The spectra were recorded in a frequency range of 100 kHz to 0.1 Hz with a perturbation amplitude of the ac voltage of 5 mV under open circuit voltage (OCV) conditions using a Metrohm Autolab PGSTAT302 N Potentiostat/Galvanostats fitted with a frequency response analyser (FRA2 module, Eco Chemie, Holland). The measurements were collected before and after charge/discharge cycles and the impedance data were plotted in a complex plane diagram, including the real part (Z') and imaginary part (Z'') of the impedance data.

2.4. Batteries and cycle performance test

A Swagelok type battery was used to investigate cycling. It had a stainless steel cylinder plunger to support a Li metal anode (Sigma–Aldrich 265985), together with an aluminium tube to allow oxygen access to the back side of the cathode. A glass microfibre filter (No. 1825-257, Whatman) separator was used, soaked in 1 M LiPF$_6$ (≥99.99%, Aldrich) in propylene carbonate (PC, Sigma–Aldrich) electrolyte. The cathode was formed by casting a mixture of carbon powder, carbon-supported catalyst, Kynar 2801 binder (Elf Atochem) and PC, together with acetone (Aldrich). The cathode was placed onto the separator and a thin open aluminium mesh (Aldrich) was placed on top to act as a current collector. The aluminium plunger was then inserted into the top of the cell and the end cap tightened to hold it in place.

The Swagelok cells were placed into glass containers. Each glass container consists of sealed vacuum tube with two Youngs' taps for gas flow and two electrical connectors (Tempatron Ltd.). The battery was gastight except for the Al mesh window that exposed the porous cathode to the O$_2$ atmosphere (1 atm pure oxygen).

All processes of assembling and dismantling the batteries were carried out in an argon atmosphere in a glove box (Unilab, MBRAUN, Germany), which provided both water and oxygen levels less than 0.1 ppm. All component parts were washed in distilled water then ethanol (agitating in an ultra-sonic bath) prior to drying at 120 °C and transfer to the glove boxes. After cell tubes were removed from the glovebox, they were placed under flowing pure oxygen (BOC) for 1 h.

Battery tests were performed in a temperature-controlled oven at 30 °C using a Maccor-4200 battery tester (Maccor). Charge–discharge curves were recorded galvanostatically at a rate of 70 mA (g carbon)$^{-1}$. The batteries were first discharged and then charged between the potential limits of 2.0 V (vs. Li/Li$^+$) for discharge and 4.3 V (vs. Li/Li$^+$) for charge.

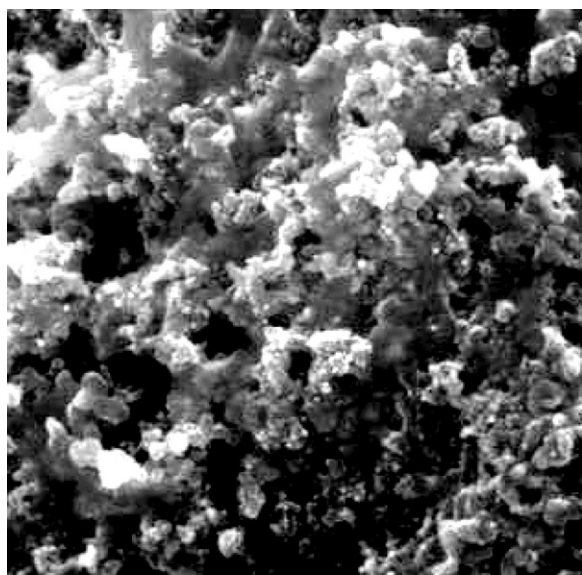## 3. Results and discussion

3.1. Surface characteristics

Surface morphologies of Pd/C and PdO/C catalyst materials were characterised for powder samples as well as composite electrode configurations. Figs. 1 and 2 compare SEM surface images of new composite cathode using a carbon-supported Pd or PdO cathode catalyst. The distribution of the Pd metal or oxide catalyst is indicated by differences in signal intensity (brightness) in the micrograph, i.e. bright parts come from the Pd metal or oxide catalyst and grey parts from carbon, binder and PC, etc. Although the image does not illustrate the particle size distribution of the Pd metal or oxide catalyst, intensity gradients show that both catalysts are well dispersed in composite electrode porous networks. In order to better understand the average particle size, at least qualitatively with respect to the supported Pd or PdO catalysts, surface morphologies of carbon-supported Pd and PdO catalyst powders were collected, as shown in Figs. 3 and 4. The carbon-supported Pd catalyst material was characterised by a rough structure with nanometric pores and complex network configuration. All Pd catalyst particles exhibit approximate spherical appearance with particle sizes smaller than 25 nm and most particles have a size of approximate 15 nm (Fig. 3). Although some features are similar as those of the Pd/C catalyst, such as roughness and porous structure and still have some catalyst sphere dimensions around 10 nm, the
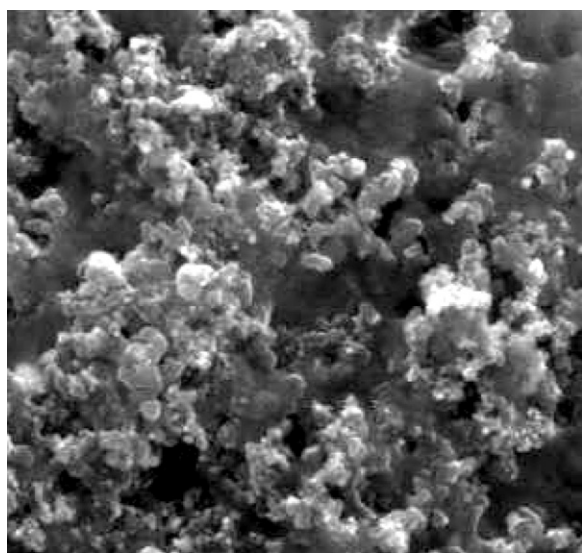
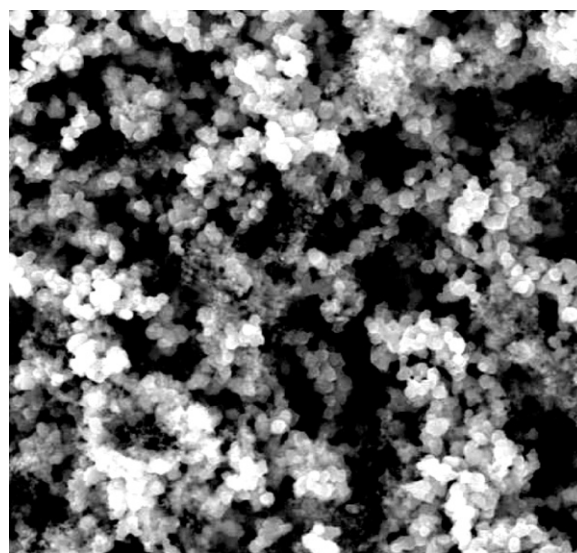**Fig. 1.** Scanning electron micrograph of the new carbon-supported Pd composite electrode at a magnification of 10,000.

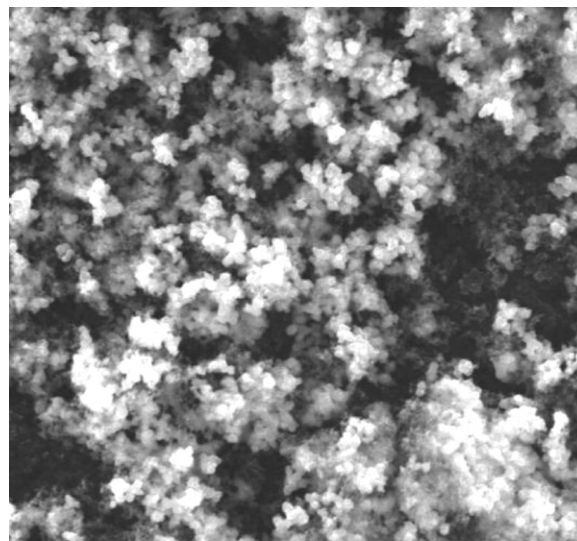**Fig. 3.** Scanning electron micrograph of the carbon-supported Pd powder at a magnification of 20,000.

morphology of the PdO/C sample changed radically, revealing the presence of catalyst (PdO)-rich cluster areas (Fig. 4). This is evidence of coalescence of PdO catalyst particles, implying that sintering phenomenon occurred for the PdO/C catalyst during the thermal synthesis process, which was different from that for the Pd/C catalyst, fabricating by the chemical synthesis. Such a difference is understandable because, as shown previously, the surface morphology of catalysts greatly depended on fabrication strategies and thermal synthesis procedure generally produced denser materials with agglomerates, than did the low temperature chemical synthesis route [14,34,15,35,36]. The implication of such a difference on the catalyst performance will be shown later.

3.2. Impedance spectra

Fig. 5 compares the Nyquist plots for new batteries with the Pd/C or PdO/C cathode catalyst obtained before the first discharge. Both impedance spectra similarly display a depressed semicircle in high frequency range (approximately from 100 to 5 kHz) with an intercept at the real axis, followed with another depressed semicircle at medium frequency (approximately from 5 kHz to 10 Hz), in addition to a straight line with an angle of approximately 45° to the real axis in the frequency range below 10 Hz. The appearance of depressed semicircles could be attributed to the dispersion of three different time constants, related to the ionic migration process in the passivating film (the high frequency range), to the charge transfer (the medium frequency range) and to the resistance of the electrolyte in the pores of the passivating film formed on the carbon (the low frequency range) [37], similar as observed from the lithium

Fig. 2. Scanning electron micrograph of the new carbon-supported PdO composite electrode at a magnification of 10,000.

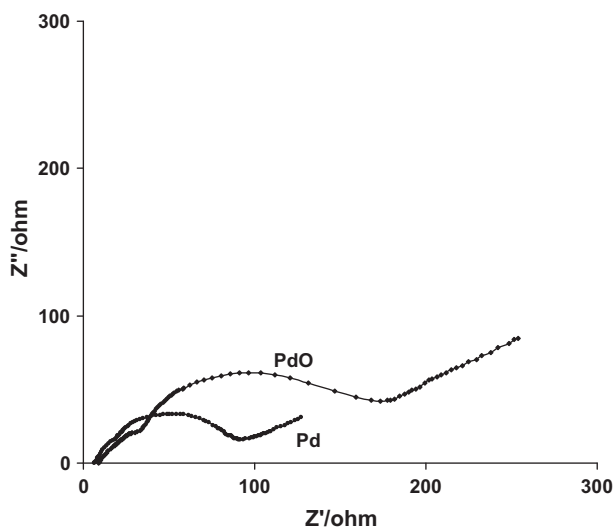**Fig. 4.** Scanning electron micrograph of the carbon-supported PdO powder at a magnification of 20,000.

Fig. 5. Impedance spectra of rechargeable Li–air batteries with carbon-supported Pd and PdO composite cathodes before cycling.

Table 2
Equivalent circuit parameters of rechargeable Li–air batteries with carbon-supported Pd and PdO catalysts.

Catalyst	R_{ex}/Ω	R_{in}/Ω	$C_{in} \times 10^6/F$	R_{ct}/Ω	$C_{dl} \times 10^6/F$	W/Ω
Pd (new)	6.2	13.5	5.7	39.2	332.1	0.12
PdO (new)	8.9	21.6	3.8	67.4	195.3	0.16
Pd* (cycle 10)	45.8	48.7	2.1	415.5	131.4	0.31
PdO* (cycle 20)	33.5	39.4	2.6	320.8	217.6	0.23

* Final cycle.

The external ohmic resistance (R_{ex}), represents a combination of the uncompensated electrolyte resistance between the air cathode and the Li anode, an electronic resistance of the current collector and contact resistances that may exist between the external surface of the electrode and the electrolyte [45,47,51,52]. The interface ohmic resistance (R_{in}) is a combination of the electrolyte resistance within the electrode, the electronic resistance of the electrode material and the contact resistance between the electrode components. The interface double layer capacitance C_{in} represents the capacity of film on the interface between the electrode and electrolyte. The charge transfer resistance (R_{ct}) indicates the resistance for electrochemical charge transfer process. The capacity C_{dl} shows the capacity related to the charge transfer process. The Warburg impedance is an indicative of the contribution from gas diffusion [45,47,51,52].

Based on this equivalent circuit, we carried out a quantitative analysis of the impedance spectra; values of the equivalent-circuit components were obtained by curve fitting using the Autolab Fra2 software and results are shown in Table 2.

3.3. Energy storage capacity

3.3.1. Initial cycle performance

Fig. 7 compares the first cycle storage performance of non-aqueous rechargeable Li–air batteries with a carbon-supported Pd or PdO cathode catalyst at a rate of 70 mA (g carbon)$^{-1}$. A unit of mAh (g cathode solids)$^{-1}$ was used in Fig. 7, although a popular unit to express specific capacity of Li–air batteries is mAh (g carbon)$^{-1}$. We believe that it may be more reasonable and more accurate to present this quantity by mAh (g cathode solids)$^{-1}$ in most cases, considering the fact that the capacity of batteries is mainly related to the quantity of active materials involved and carbon is not only active material; each compo-

electrode interface [38–41] or from the carbon/organic electrolyte interface [42–44]. The linear part was associated with the diffusion of electrochemical active ionic species within electrode porous network, including the interface between surface films, the catalyst and its carbon support as well as the capacitive effect of the carbon [45–47]. The straight low frequency line with a phase angle of about 45° in Fig. 5 implies the involvement of diffusion control, due to the slow diffusion of electroactive species across the interface between surface films and the catalyst supported carbon along the pores in the air cathode (Warburg effect) [45,46].

The large difference in impedance response for both batteries was also noticed. As reported previously, the major source of battery impedance came from the cathode and the Li anode had only a weak contribution to the whole battery system for both Li-ion and Li–air batteries [45,47–49]. Therefore, the observed impedance differences can reasonably attributed mainly to the cathode difference. For instance, the depressed semicircle appeared in the low-frequency range mainly to cathode effects, i.e. a contribution from the inter-particle contacts such as catalyst–catalyst, carbon–catalyst and carbon–carbon grain contacts, within the composite cathode [45,48,49]. In spite of such a great variation, an equivalent circuit proposed for and confirmed in Li–O$_2$ batteries [45,48,50] can be used to fit the spectra of our batteries because of similar battery structures and similar shapes of spectra generated from such batteries, which is shown in Fig. 6. The equivalent circuit consists of an external ohmic resistance (R_{ex}), an interface ohmic resistance (R_{in}), a charge transfer resistance (R_{ct}), double layer capacitances (C_{in} and C_{dl}) and a Warburg (W) impedance.
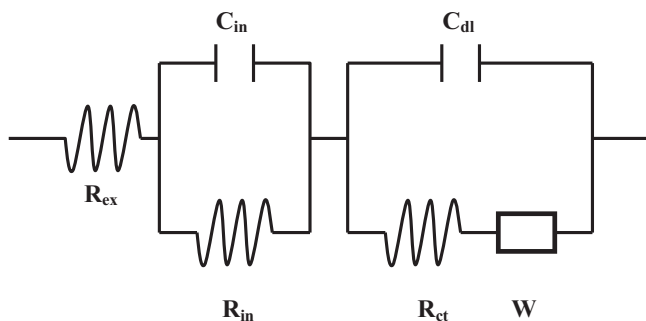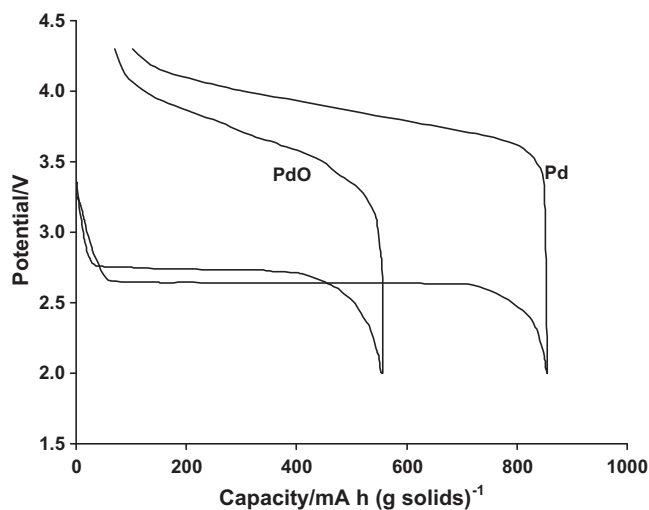

Fig. 6. The equivalent circuit of rechargeable Li–air batteries with carbon-supported Pd and PdO composite cathodes.

Fig. 7. Variation of potential with state of charge for rechargeable Li–air batteries with carbon-supported Pd and PdO composite cathodes. The first cycle, which was cycled at a rate of 70 mA (g carbon)$^{-1}$ between 2.0 and 4.3 V. Temperature: 30 °C.

nent has its irreplaceable role. When a metal or oxide catalyst co-exists, carbon is not even the most important active material. As shown in Fig. 7, although both catalytic materials produced similar shaped potential–capacity curves, they were quite different in discharge capacities and in charging/discharging potentials. The battery with the Pd/C cathode catalyst delivered higher specific capacity (ca. 855 mAh (g solids)$^{-1}$) than that with the PdO/C catalyst (ca. 556 mAh (g solids)$^{-1}$). Discharging for the battery with the Pd/C catalyst started at a voltage of 2.65 V with subsequent charging occurred at 3.40 V. In contrary, the battery with the PdO/C cathode catalyst had a higher discharging voltage (2.75 V) but lower charging voltage (3.15 V).

3.3.2. Discussion

The electroreduction of molecular oxygen involves the dissociative absorption of oxygen by a strong interaction between catalysts and oxygen and a redox reaction of the catalyst site. Consequently, activity of an electrocatalyst for the oxygen reduction reaction greatly depends on its ability for dissociative absorption of oxygen. In our non-aqueous environment within the lithium–O_2 battery, discharge products could be Li_2O_2 from partly breaking the di-oxygen bond, i.e. the reduction of O_2 to O_2^{2-}, followed by its subsequent oxidation [3,4,53,54]:

$$2Li + O_2 \leftrightarrow Li_2O_2 \qquad (6)$$

Since the discharge voltage of a Li–air battery is an indication of its ORR activity of the cathode catalyst, higher discharge voltage of the battery with the PdO catalyst, compared with that with the Pd counterpart (Fig. 7), reflected its superior ORR activity to the Pd.

On the other hand, other physical and chemical properties of the catalytic materials, e.g. porosity, directly affect the discharge capacity of the Li–air batteries. During cycling processes of the lithium–O_2 battery, not only Li_2O_2 was formed, as shown in Eq. (6), further reactions were possible, such as [54]:

$$Li_2O + CO_2 \rightarrow Li_2CO_3 \qquad (7)$$

The formation and transfer of these insoluble substances hinted that the difference in surface characteristics of two catalysts, as mentioned above, could play a great role in their battery performance. Some clues can be drawn from our SEM and impedance data and the performance difference may result from:

(i) Difference in surface morphology

It is widely accepted that chemical and physical properties of catalysts are strongly affected by the change of particle dispersion and particle size [18–20,55]. Catalysts with high dispersion values show lower polarisation than bigger size catalysts [18–20]. Size decrease of catalyst particle is believed to increase the proportion of the total number of catalyst atoms lying near to or on the surface, making the electrochemical reactivity of the particles more and more important, thus enhancing their electrochemical activity towards a catalytic reaction [18–20,55]. In a battery, cathodes with higher surface area could deliver a better discharge performance than with a lower surface area due to the decreased diffusion path length, as a consequence of the presence of very small particles [56].

In our case, qualitatively, we can see a higher dispersion of the Pd/C catalyst than the PdO/C catalyst in composite electrode configurations, as used in our Li–air batteries (see Figs. 1 and 2). This can be more clearly identified in Figs. 3 and 4, where cluster-like PdO catalyst particle groups were formed during the thermal synthesis process (Fig. 4) while the Pd particles revealed more uniform distribution in the carbon support matrix (Fig. 3). Further evidence regarding particle size was obtained from TEM measurements where higher
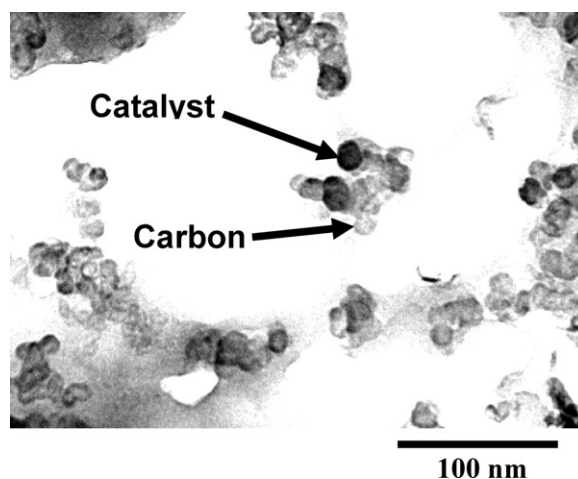

Fig. 8. Transmission electron micrograph of the carbon-supported Pd composite electrode at a magnification of 13,5000.

magnifications could be used. For example, at a high magnification of 130,000×, the nanoporous structure of each Pd particle is revealed for the composite electrode with the Pd/C catalyst (Fig. 8). The Pd particles, most of them with dimensions approximately between 5 and 10 nm, were distributed in composite networks, made up of carbon, Kynar binder and PC. The TEM image for the composite electrode with PdO/C catalyst (Fig. 9) was rather different from that with the Pd catalyst. Although individual PdO particle with small particle sizes around 5–10 nm can be seen, significant number of PdO particles was agglomerated and their dimensions were around 20 nm (Fig. 9). As a general rule, the bigger the particle, the smaller the electrochemical active surface area [57,15]. This means that the Pd/C catalyst has larger active surface area than its PdO counterpart, in addition to higher dispersion. The large surface area of catalyst could result in a larger contact surface between reactant oxygen molecules, electrolyte and binder, and thereby enhance any reactions between them. These factors could be accounted for their different initial performance, as shown in Section 3.2.

(ii) Their difference in initial resistance

As a semiconductor, PdO has lower conductivity than Pd metal [58–60]. More importantly, in a composite electrode network, both catalysts had different combinations with other
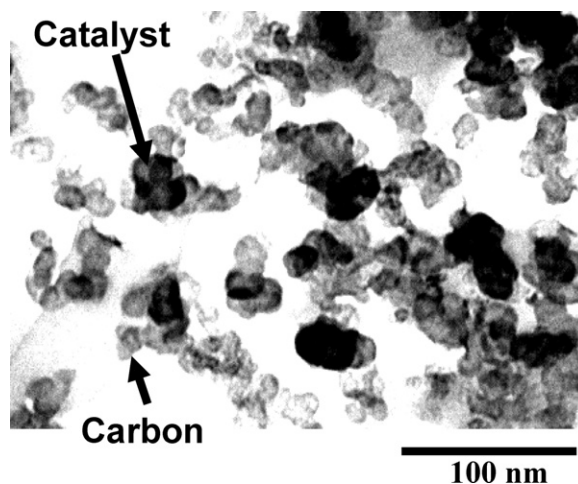

Fig. 9. Transmission electron micrograph of the carbon-supported PdO composite electrode at a magnification of 13,5000.

components due to their differences in volume, bonding energy and structure etc. This had great impact on the electrode conductivity. These arguments were also confirmed by our impedance data, which were collected in situ of two Li–air batteries with the Pd/C or PdO/C cathodes, otherwise under identical conditions, as shown in Fig. 5 and Table 2. It is easily seen from Fig. 5 that the battery with the Pd/C cathode had a lower external ohmic resistance (R_{ex}, i.e. the high frequency intercept at the real Z-axis) than that with the PdO/C, i.e. 6.2 vs. 8.9 Ω (Table 2). The same trend was observed for interface and charge transfer resistances, ca. 13.5 vs. 21.6 Ω and 39.2 vs. 67.4 Ω (Table 2). Such a difference in resistances led to the superior initial performance of the battery with the Pd/C cathode to that with the PdO/C. For example, since the medium frequency impedance mainly reflects the contribution of the ionic diffusion from the bulk of electrolyte to the reaction sites gas diffusion [45,51], so a lower charge transfer resistance means better ionic diffusion.

(iii) Their difference in other initial electrochemical properties

As displayed in the impedance data, higher capacities were observed for the battery with the Pd/C cathode, compared to that with the PdO/C (Table 2). In general, the capacitance that appeared in complex plane impedance plots can be taken as a measure of total active area, which is proportional to the electrochemically accessible surface area of the electrode [61,62]. Therefore, the battery with the Pd/C cathode showed better performance than that with the PdO/C due to more accessible active sites. It should be stated that the capacitance observed in impedance spectroscopy includes double-layer capacitance and Faradaic pseudo capacitance terms for both the catalyst and carbon surfaces of the catalyst particles. Also, relative contributions to total capacitance from the catalyst and carbon surfaces or from double-layer and Faradaic capacitance changed with different electrodes. Due to the difficulty to separate these terms, in practice, it can be reasonably assumed that their relative contributions to the total capacitance do not vary greatly between different electrodes and thus the total capacitance is still a reasonable relative measure of the electrochemically active area, as proved in other catalytic systems [61].

Warburg impedance was also different for both batteries and lower Warburg impedance for the battery with the Pd/C cathode indicates its lower diffusion resistance than that with the PdO/C cathode (Table 2).

It is worthwhile to state that propylene carbonate (PC) was selected initially in our project due to the fact that it is one of preferred solvents for commercial lithium-ion batteries due to its lower volatility and higher flash point. It is true that there are downsides of PC, for example, it has high reactivity towards the bare Li metal and PC itself is easily decomposed during charging process, which led to substantial formation of insulating film during reduction, consisting of Li_2CO_3, Li_2O_2, Li_2O and LiOH, plus other PC reduction products, such as $CH_3CH(OCO_2Li)CH_2$–OCO_2M, CH_3CHOCO_2Li and CH_3CHOLi [4,65–70]. It is possible that these downsides had some negative effect on displaying the catalyst behaviour to some extent. However, we believe that such an effect was limited under our conditions, since we could clearly distinguish the intrinsic cycling stability of batteries with different cathode catalysts, even in the presence of the electrolyte decomposition. These observations showed that such a masking effect, if there was any, should not significantly affect the comparability of both Pd and PdO catalysts under other comparable conditions. Indeed, with more intensive studies, we and other groups have recognised the neces-
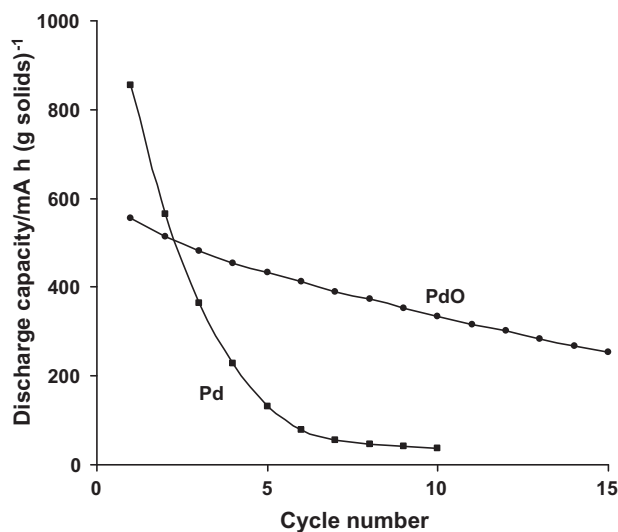

Fig. 10. The cycle performance (discharge capacity against cycle number) of the rechargeable lithium–oxygen batteries with carbon-supported Pd and PdO composite cathodes. Batteries were cycled at a rate of 70 mA (g carbon)$^{-1}$ between 2.0 and 4.3 V. Temperature: 30 °C.

sity to search PC alternatives. Investigation in this field has made progress and related results will be published later.

3.4. Stability

In practice, battery stability, which can be measured by retention of discharge capacity on cycling, is more important than its initial performance. As reported previously, the most challenge issue for Li–air batteries is their capacity retention ability [1,3,5,14]. This mainly depends on how long the cathode catalyst can survive as active component in a composite network under severe charging/discharging cycles.

3.4.1. Capacity retention ability

Fig. 10 compares the variation of discharge capacity on cycling for the rechargeable lithium–oxygen batteries with Norit carbon black-supported Pd and PdO cathode catalysts. Both batteries experienced performance deterioration but with quite different decrease rate. The capacity of the battery with the Pd catalyst fell rapidly from around 855 mAh (g solids)$^{-1}$ to a low value of 132 mAh (g solids)$^{-1}$ after 5 cycles, corresponding to a capacity retention of 3.1% per cycle (Table 3). At the 10th cycle, the discharge capacity was even lower to just 38 mAh (g solids)$^{-1}$ with a low capacity retention of 0.44% per cycle (Table 3). In contrast, the battery with the PdO catalyst displayed much higher capacity retention ability, e.g. the capacity retention was still 6% per cycle at the 10th cycle. The data suggested that the PdO catalyst was more stable than the Pd catalyst under repeated cycling conditions.

3.4.2. Discussion

The capacity loss of a positive electrode during cycles is a common phenomenon for lithium batteries as a result of loss and deterioration of the active material and the decrease in conductivity between the active material and the collector [8]. In our case, as mentioned in the last section, our Li–air batteries with both Pd/C and PdO/C cathode catalysts could not maintain their initial high capacities. Several aspects may be responsible for the performance deterioration with charge/discharge cycling:

(i) The loss of the active material of the cathode

Table 3
Charge/discharge voltages and discharge capacities of rechargeable Li–air batteries with carbon-supported catalysts.

Catalyst	Charge voltage[a](V)	Discharge voltage[a](V)	Capacity[a](mA h g^{-1})	Capacity[b](mA h g^{-1})	Capacity retention per cycle[b](%)
Pd	3.40	2.65	855	38	0.44
Pt	3.55	2.72	616	279	4.53
Ru	3.70	2.76	577	65	1.13
PdO	3.15	2.75	556	336	6.04
RuO$_{2.0}$	3.65	2.89	446	234	5.25
MnO$_{2.0}$	3.80	2.51	807	626	7.76

[a] Data for the first cycle.
[b] Data for the 10th cycle.

Under severe cycling conditions, the oxidation (e.g. Pd catalysts) and/or reduction (e.g. PdO) of catalysts could be occurred. This led to the decrease in active sites, lowering cathode catalytic activity. Qualitatively, we could see obvious loss of the cathode solid materials from glass fibre supports. Weighing our cathodes before and after test quantitatively confirmed the material loss, which definitely led to loss of catalytic activity of the cathode. As a direct consequence of such a material loss, the increased gaps between the active material and the collector were observed; some loose materials were formed in such gaps. This could increase the battery resistance.
(ii) The agglomeration of catalyst particles and other cathode components, as shown in our SEM data later. This caused reduction in electrochemical active surface area and increased diffusion resistance.
(iii) The loss of solvent (PC)
  The loss of PC solvent and the formation of white solid substances were observed after charge/discharge cycling. There were several possible reactions or processes that are responsible for such a loss. For instance, as mentioned above, owing to high reactivity of PC towards the bare Li metal and PC itself is easily decomposed during charging process, which led to substantial formation of insulating film during reduction, consisting of Li_2CO_3, Li_2O_2, Li_2O and LiOH, plus other PC reduction products, such as $CH_3CH(OCO_2Li)CH_2$–OCO_2M, CH_3CHOCO_2Li and CH_3CHOLi [3,54,63–68]. Further reactions could occur in the presence of carbon dioxide and moisture, such as that described in Eq. (7) and:

$$2LiOH + CO_2 \rightarrow Li_2CO_3 + H_2O \qquad (8)$$

This affected contact between catalyst particles, carbon support particles and binder, leading to the decreased tightness between electrodes, separator and current collectors, which thus reduced the battery conductivity. The PC loss also had a negative impact on transport of Li ion and intermediates. As a consequence of the loss of their existing media, Li ion transfer could be severely prevented and/or blocked, which could limit the involvement of active components (such as Li ion) and greatly reduce the battery performance. Further more, as mentioned above, it was possible that insoluble substances generated, such as Li_2O_2 and Li_2CO_3 [4,54]; they could not diffuse away rapidly enough from the surface. They might be adsorbed to the surface of the catalysts and block the active sites for further dissociative absorption of oxygen.

A comparison of the impedance spectra shown in Fig. 5 with Fig. 11 and data in Table 2 confirmed above qualitative observations. A significant increase in resistances and reduction in capacities was clear, for example, the external resistance increased from 6.2 to 45.8 Ω and from 8.9 to 35.5 Ω for the battery with the Pd/C and PdO/C cathode catalyst, respectively (Table 2). Such a change in electrochemical properties of the cathodes caused dramatic performance deterioration.

It should state that there was uncertainty concerning the solvent loss and further study using more accurate techniques would benefit to understand this qualitative observation.

Moreover, as shown above, our Li–air batteries with Pd/C and PdO/C cathode catalysts did exhibit different deterioration rates. As the only difference of two batteries was their cathode catalysts, so cycle ability shown here is a sign of activity retention of cathode catalysts during charge/discharge cycling operation. The following aspects may be responsible for such a difference in capacity fading:

(i) Intrinsic stability
  In general, under the conditions of catalysis, it is expected that the metal surface will indeed be in a dynamic 'living' state with the tendency to form oxide, which destabilises the metal surface and represent metastable precursors for the phase transition to a more stable surface-oxide [69]. For this reason, even industrial Pt–Ru catalysts are not simply bimetallic alloys, but contain hydrous Ru oxide and RuO_2 oxide is more stable [69,70]. For Pd catalysts, the interaction of oxygen with Pd is very easy; exposure of Pd surfaces to O_2 even at or below room temperature leads to dissociation of molecular oxygen, forming a chemisorbed layer of oxygen atoms. Such a unique property made the activity of Pd catalysts extremely sensitive to the catalyst history and formation of an unstable surface structure with a lower Pd atom density is a natural first step consequently, followed by the stable PdO formation [23,71,72]. On the contrary, PdO is very stable even at high temperature [73]. As the most stable species of oxygen-containing palladium compounds, PdO is more stable than Pd itself, which was already demonstrated in oxygen reduction and other catalytic reactions [23,72,74]. The stability of PdO electrode during oxy-
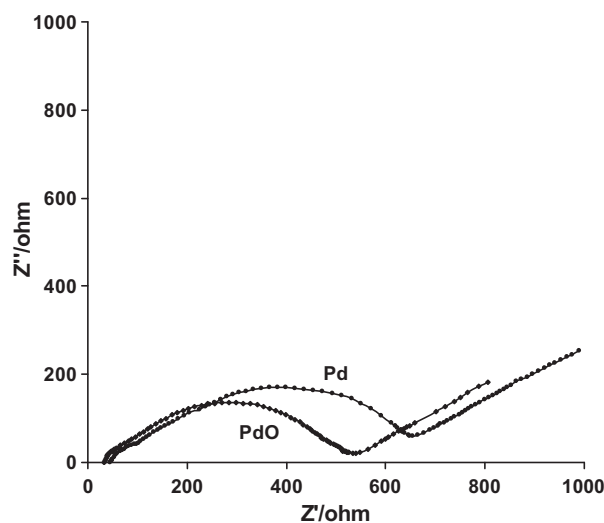

Fig. 11. Impedance spectra of rechargeable Li–air batteries with carbon-supported Pd (cycle 10) and PdO (cycle 20) composite cathodes after the final cycle.
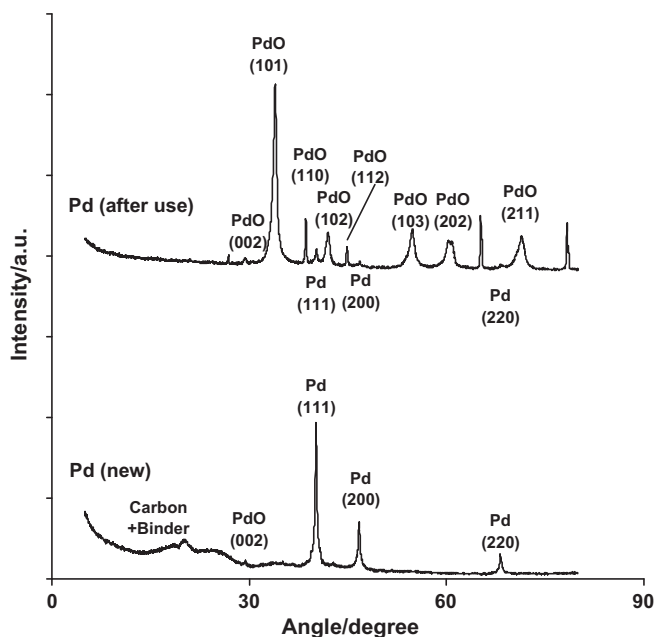
Fig. 12. X-ray powder diffraction patterns of the carbon-supported Pd composite cathode: (a) before cycling and (b) after the final cycle (cycle 10).
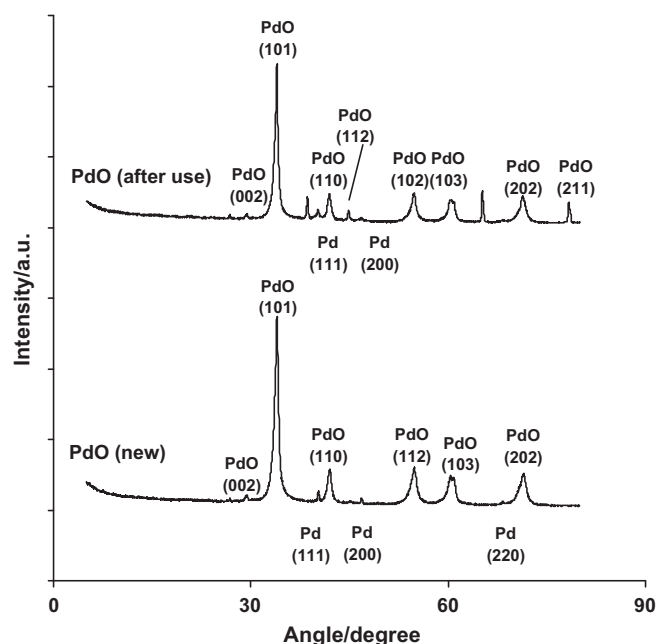

Fig. 13. X-ray powder diffraction patterns of the carbon-supported PdO composite cathode: (a) before cycling and (b) after the final cycle (cycle 20).

gen reduction in aqueous media was confirmed previously and its surface morphology and cyclic voltammograms had only a small change [75]. The palladium oxide showed higher stability than palladium metal during oxygen reduction in aqueous acid environment [22]. While surface composition of the palladium oxide remained unchanged, the Pd metal gradually disappeared and the PdO increased concomitantly. As a result, the stability of the Pd cathode during oxygen reduction was enhanced [22]. Another example was the improved catalyst durability during oxygen reduction reaction owing to oxidation treatment of Pd and Pd–Co alloy electrodes [76]. This was attributed to the presence of surface PdO species, which were able to protect the Pd catalyst from structural changes as well as hinder the dissolution of hydrogen into bulk Pd/C [76].

Higher stability of the PdO catalyst under our battery cycling conditions, compared with the Pd catalyst, was confirmed by our XRD data (Fig. 12). A comparison of XRD patterns for the Pd composite electrodes before and after charge/discharge cycling, i.e. curves "Pd (new)" and "Pd (after use)" in Fig. 12, exhibits a significant decrease in intensity of main Pd peaks, i.e. Pd (1 1 1), Pd (2 0 0) and Pd (2 2 0). Meanwhile, apart from the increased intensity of PdO (0 0 2) that existed in the new Pd sample, new PdO peaks appeared after charge/discharge cycling, i.e. PdO (1 0 1), PdO (1 1 0), PdO (1 0 2), PdO (1 1 2), PdO (1 0 3), PdO (2 0 2) and PdO (2 1 1). On the contrary, the PdO composite electrodes showed less dramatic change in XRD patterns; main PdO peaks, i.e. PdO (1 0 1), PdO (1 1 0), PdO (1 1 2), PdO (1 0 3) and PdO (2 0 2), were maintained, in addition to two new PdO peaks, i.e. PdO (1 0 2) and PdO (2 1 1), after the cycling operation (Fig. 13). The evidence suggests that PdO is more stable than Pd and could deliver superior catalytic activity towards oxygen reduction to the Pd catalyst under severe battery cycling conditions. As a result, the Pd/C cathode could not maintain its initial high activity; the performance of the battery with the Pd/C catalyst deteriorated at a greater rate, compared to that with the PdO/C catalyst (Fig. 10).

(ii) Surface morphology change

The rapid and relatively slow deterioration of our batteries with Pd/C and PdO/C cathode catalysts was also a direct consequence of their cathode surface changes. Examples are shown in Figs. 14 and 15, which show SEM images of the Pd/C and PdO/C cathode catalysts after experiencing charging/discharging cycling. Although the images do not well illustrate the particle size distribution of both catalysts, intensity gradients show some remaining dispersed catalysts (bright points and/or areas). Significant changes in the distribution of both catalysts and their particle sizes were observed, compared with new electrodes (Figs. 1 and 2). In spite of both cathode surfaces exhibiting irregular shapes and porous structures after charging/discharging cycles, their agglomeration extent and catalyst distribution did show some differences (Figs. 14 and 15). The PdO/C catalyst displayed a lower degree of agglomeration and better catalyst dispersion, characterised by smaller cauliflower-like agglomerates and rougher surface
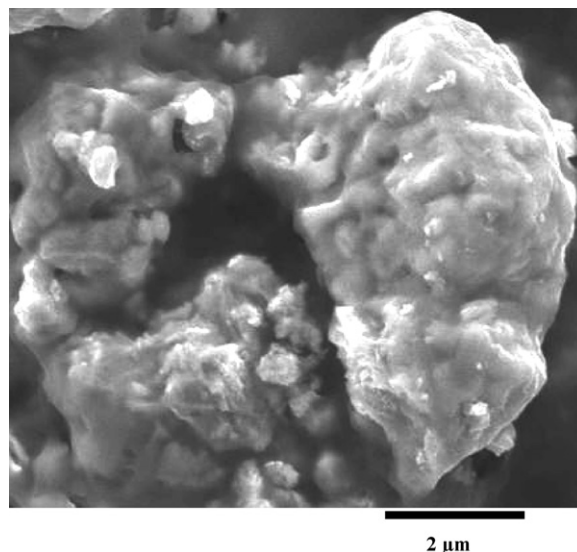

Fig. 14. Scanning electron micrograph of the carbon-supported Pd composite electrode after charge/discharge cycling at a magnification of 10,000.
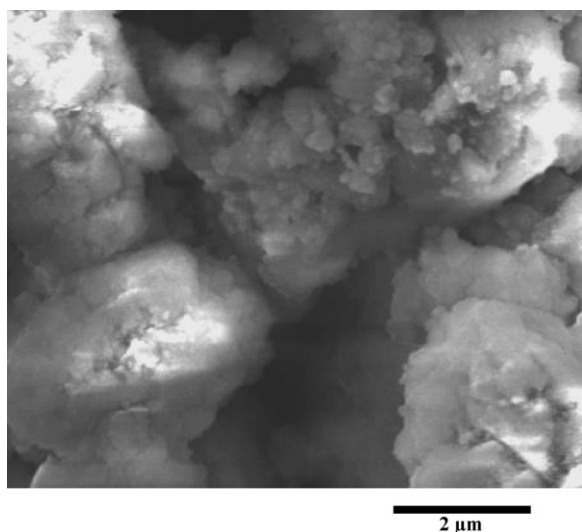
Fig. 15. Scanning electron micrograph of the carbon-supported PdO composite electrode after charge/discharge cycling at a magnification of 10,000.

Fig. 16. Variation of potential with state of charge for rechargeable lithium–oxygen batteries with carbon-supported Pt, Ru, RuO_2 and MnO_2 composite electrodes. The first cycle, which was cycled at a rate of 70 mA (g carbon)$^{-1}$ between 2.0 and 4.3 V. Temperature: 30 °C.

(Fig. 15), compared with the Pd/C catalyst (Fig. 14). Moreover, relatively small catalyst particles could still be seen for the PdO/C catalyst (Fig. 15) than that for the Pd/C catalyst (Fig. 14). These differences mean that the PdO/C catalyst had larger electrode active surface area than the Pd/C catalyst, thus, produced lower degradation rates and better discharge performance, as reported in other types of batteries [56].

The most striking feature for both electrodes is their severe agglomeration. Most pores for new electrodes (Figs. 1 and 2) were nearly eliminated, replaced by big blocks and cauliflower-like agglomerates made up catalyst, carbon and binder particles (Figs. 14 and 15). The implication of such a drastic structure change is the great reduction of the interface between the catalyst phase, carbon support and binder, as a result of the decreased pores and the formation of enlarged blocks. Therefore, catalyst, catalyst support and binder could not function properly, affecting catalyst activity and diffusion of reactants (oxygen), intermediates (such as dissociative absorbed oxygen) and products (such as Li_2O_2).

Severe aggregation of catalyst particles was also observed and particle sizes increased from around 10–20 nm (Figs. 1 and 2) to approximately 100–500 nm (Figs. 14 and 15). One direct result of such a change is the drastic reduction in electrochemical active sites due to less catalyst atoms near to or on the surface and an incorporation of part of catalyst atoms from the surface into the bulk [55,79], leading to a great decrease in the battery capacity. Even for remaining catalyst active sites, the diffusion path length increased due to the catalyst agglomeration and surface area reduction. This would make them difficult to be accessed by reactant oxygen molecules as well as for diffusion of intermediates (such as dissociative absorbed oxygen) and products (such as Li_2O_2) more difficult. Consequently, the catalyst activity decreased and the batteries suffered from unstable deteriorating performance.

(iii) Difference of changing electrochemical properties, such as resistance and capacitance

A comparison of Fig. 11 with Fig. 5 and related values in Table 2 exhibits different deterioration rates for the Li–air battery with Pd/C or PdO/C cathode catalyst. The latter showed smaller increase in resistances and lower decrease in capacitances than the former. Although the battery with the PdO catalyst stood up to more charging/discharging cycles, it showed lower resistances and higher capacities, compared
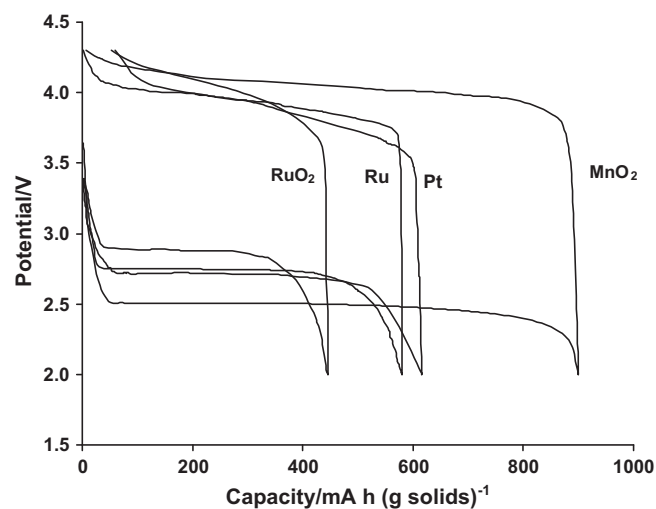
with that with the Pd/C cathode, e.g. 320.8 vs. 415.5 Ω in charge transfer resistance and 2.2×10^{-4} vs. 1.3×10^{-4} F in charge transfer capacitance. These differences in electrochemical property determined the better retention of the battery with the PdO catalyst than that with the Pd/C catalyst.

Overall, it seems reasonable to assume that the cycling ability of the batteries largely depended on the ability of catalysts to support insertion and removal of lithium via the reversible reaction (6). In this respect, the PdO/C catalyst exhibited quite good recovery ability and may play an active role in removal of lithium oxides during discharge/charge cycling. It may worth stating that we have no intention to compare the Li–air battery with the Li–ion battery here. Even with the same cathode material, the performance of such a material in the Li–air batteries and their Li–ion counterparts is not totally comparable due to its function differences, although such a cathode in these batteries has some similar role at least.

3.5. Comparison with other metal and oxide catalysts

It is worth comparing the Pd and PdO catalysts with other popularly used catalysts, such as Pt – the best cathode catalyst for fuel cells [78–80] and MnO_2 – (the most promising cathode catalyst for Li–air batteries [3,14].

All of our batteries had the identical electrode construction except for cathode catalyst itself. This made our results from different catalyst materials comparable.

3.5.1. The first cycle

Fig. 16 shows storage performances of rechargeable Li–air batteries with carbon-supported Pt, Ru, RuO_2 and MnO_2 cathode catalysts at a rate of 70 mA (g carbon)$^{-1}$. Although these materials produced similar shaped potential–capacity curves as those for the batteries with the Pd/C and PdO/C catalysts, they were quite different in discharge capacities and in charging/discharging potentials. Table 3 summarises key data for these batteries and compares to those collected from batteries with the Pd/C and PdO/C catalysts. The largest specific capacity of the first cycle was delivered by the battery with the Pd/C cathode catalyst, i.e. 855 mAh (g solids)$^{-1}$, and the smallest capacity was obtain with the RuO_2/C catalyst, which was only 446 mAh (g solids)$^{-1}$.
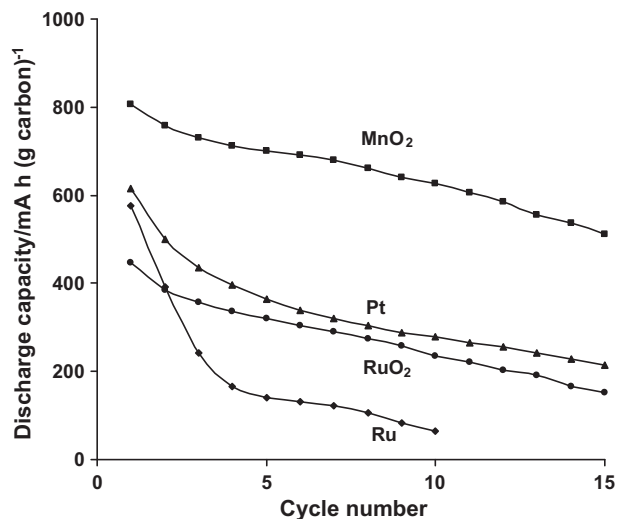
Fig. 17. The cycle performance (discharge capacity against cycle number) of rechargeable lithium–oxygen batteries with Pt, Ru, RuO$_2$ and MnO$_2$ composite cathodes. Batteries were cycled at a rate of 70 mA (g carbon)$^{-1}$ between 2.0 and 4.3 V. Temperature: 30 °C.

As mentioned before, different activities of cathode catalysts for oxygen reduction determined the discharge capacity of their batteries. Thus, based on the first cycle data, the Pd/C cathode catalyst was the most active cathode catalyst, as shown by its highest discharge capacities.

As can be seen, the catalyst materials not only affected the discharge capacity, but also caused diverse discharging and charging potentials. The battery with the MnO$_2$/C catalyst had the lowest discharge voltage (2.51 V) but subsequent charging occurred at the highest charge voltage, i.e. 3.80 V. The highest discharging voltage belonged to the battery with the RuO$_2$/C catalyst (2.89 V) and the lowest charging voltage (around 3.15 V) was for that with the PdO/C catalyst. The reason for termination of the discharge process was increased polarisation because solid Li$_2$O$_2$ were formed and filled the pores, which is also a major factor influencing the retention of our batteries [3]. Hence, charging potential can be taken as one of criteria, apart from discharge capacity, to measure catalyst activity. In this regard, both Pd and Pt catalysts were marginally better than the Ru catalyst, whist the RuO$_2$ gave the greatest discharge voltage of all catalysts examined.

3.5.2. Cycle ability

Fig. 17 shows variation of the retention of discharge capacity on cycling for rechargeable lithium–oxygen batteries with metal and oxide catalysts. Qualitatively, the battery with the MnO$_2$/C cathode catalyst exhibited the best stability and that with the Pd/C the least stable in terms of capacity loss with cycling. More data are shown in Table 3. It is interesting to notice that all batteries with the oxide cathode catalysts displayed better cycle ability than those with the metal counterparts. For instance, at cycle 10, the battery with the MnO$_2$/C catalyst showed the most stable performance, with the highest capacity retention of 7.76% per cycle. At the other extreme end, the battery with the Pd/C catalyst exhibited the lowest capacity retention of 0.44% per cycle.

3.6. Summary: which is better—metal or oxide?

As shown above, batteries with metal catalysts could deliver better initial discharge capacities with higher discharge potentials but inferior retention, compared to their oxide counterparts. For example, at cycle 10, all batteries with the oxide catalysts showed better capacity retention than those with the metal catalysts. Since the main barrier for achieving practical application of rechargeable Li–air batteries to electric vehicles is their cycle life, the battery cycling ability at required current levels is a more important criterion than the initial performance to select cathode catalysts for rechargeable Li–air batteries. In this regard, oxides appear more favourable than metal as catalyst for the rechargeable Li–air battery.

It may worth stating that comparison of the performance between the bulk catalysts and nanoscale catalysts has not been carried out yet in this work, although this should provide more insightful information and is worthwhile to do in further research. It is also important to know the surface chemistry of pristine catalysts, e.g. Pd and PdO catalysts. For the Pd catalyst used in this work, even some measures were adopted, the Pd catalyst surface still existed trace oxides, as shown in the XRD data. Further effort is required to produce pristine Pd catalyst in order to thoroughly understanding the catalyst behaviour. Although every effort was made to understand the difference of metal and oxide catalysts, even for the Pd/PdO couple, there was more to do to thoroughly understand the catalyst behaviour. It should be cautious when study other metal/oxide couples due to complexity and differences between each couple. Moreover, it should state that the cut off voltage is one of main parameters affecting battery behaviour. In our case, the same trend was observed when batteries with the PdO and Pd catalysts were cycled to either 4.0 or 4.3 V. However, this may not be the case for other catalysts. For instance, the electrolyte decomposition potential on Pt surface could be significantly lower than that of MnO$_2$. Therefore, cut off voltages should be carefully chosen for different catalysts to avoid major electrolyte decomposition.

For a catalytic material involved carbon support, it is well worth counting role of carbon species, particularly considering the conditions to fabricate the carbon-supported catalytic materials, e.g. oxidised in air at 550 °C for PdO/C. It was well known that the reactivity of a carbon is influenced not only by impurities and by surface oxide but also by the heat treatment (or carbonisation) temperature employed in its preparation [81]. The original idea for treating PdO/C at high temperature (500–550 °C) under air atmosphere was to improve structure (e.g. porosity) and electrochemical properties of the catalyst material via surface species changes and removal of impurities while there is little loss in carbon itself, which had been demonstrated previously [28–32,35]. Under such conditions, e.g. at 550 °C, carbon surface oxides could be formed [81]. These carbon surface oxides showed greater stability at the lower reaction temperature [81]. Such surface changes may be one of reasons for the improved electrochemical properties (both activity and stability) of carbon treated at high temperature in air atmosphere [28–32]. Moreover, as observed previously, when the carbon samples were heated at about 550 °C, apart from decomposing some of the surface oxide into a mixture of carbon monoxide and carbon dioxide, new catalytic free-radical centres was formed, consisting of semi-quinone, carboxyl or single bonded peroxide, in which the unpaired electrons are localized on oxygen atoms. Unpaired electron concentrations show a maximum, usually at carbonisation temperatures in the range 550–600 °C [81,82]. Thus, these surface carbon oxides could play some roles in electron transfer, although we have not completely understand these roles yet. This is an interesting topic for further research, which has been addressed in our ongoing studies. Furthermore, our data confirmed that catalyst itself played more important roles than carbon and surface oxides during the charge/discharge cycling process. For example, capacities for batteries with purified oxidised carbon and non-oxidised carbon cathode were only 10–20% of those with PdO/C. Even worse, the batteries with carbon-only cathodes could only cycle less than 5 cycles. It is apparent that a catalyst is necessary to promote decomposition of Li$_2$O$_2$ on charging as well as aids the formation of Li$_2$O$_2$ on discharge.

Overall, there was more to do to thoroughly understand the catalyst behaviour, even for the Pd/PdO couple, although every effort was made to understand the difference of metal and oxide catalysts in this work. It should be cautious when study other metal/oxide couples due to complexity and differences between each couple.

4. Conclusions

A study of rechargeable Li–air batteries with model Pd/C and PdO/C cathode catalysts demonstrated that the charging/discharging cycle ability is the most important criterion for catalyst selection, although the initial battery performance cannot be ruled out as a reference guide. Performance deterioration was observed for batteries with both catalysts, this is partly due to their activity loss as a consequence of the catalyst agglomeration and electrode structure changes, which led to decrease in electrochemical active area and in active sites accessible for oxygen molecules as well as increase in diffusion resistance. However, the battery with the PdO/C catalyst showed greater capacity retention than that with the Pd/C catalyst. The performance difference of both catalysts was closely related their intrinsic catalytic activities for oxygen reduction, stability and surface change during charge/discharge cycling.

A comparison of both catalysts with other metal and oxide catalysts (Pt, Ru, RuO_2 and MnO_2) under charge/discharge conditions confirmed that, as a general rule, oxides are better cathode catalysts than their metal counterparts for rechargeable Li–air batteries.

Acknowledgements

References

[1] M. Armand, J.-M. Tarascon, Nature 451 (2008) 652.
[2] P.G. Bruce, Solid State Ionics 179 (2008) 752.
[3] A. Debart, J.L. Bao, G. Armstrong, P.G. Bruce, J. Power Sources 174 (2007) 1177.
[4] T. Ogasawara, A. Debart, M. Holzapfel, P. Novak, P.G. Bruce, J. Am. Chem. Soc. 128 (2006) 1390.
[5] K.M. Abraham, Z. Jiang, J. Electrochem. Soc. 143 (1996) 1.
[6] H. Baughman, A.A. Zakhidov, W.A. de Heer, Science 297 (2002) 787.
[7] F. Raimondi, G.G. Scherer, R. Kotz, A. Wokaun, Angew. Chem. Int. Ed. 44 (2005) 2190.
[8] M.S. Wu, P.J. Chiang, J.T. Lee, J.C. Lin, J. Phys. Chem. B 109 (2005) 23279.
[9] E.S. Toberer, T.D. Schladt, R. Seshadri, J. Am. Chem. Soc. 128 (2006) 1462.
[10] H. Zhang, G.P. Cao, Y.S. Yang, Z.N. Gu, J. Electrochem. Soc. 155 (2008) K19.
[11] M.M. Thackeray, W.I.F. David, P.G. Bruce, J.B. Goodenough, Mater. Res. Bull. 1 (1983) 461.
[12] H. Kawaoka, M. Hibino, H.S. Zhou, I. Honma, J. Power Sources 125 (2004) 85.
[13] Y.-C. Lu, H.A. Gasteiger, M.C. Parent, V. Chiloyan, S.-H. Yang, Solid State Lett. 13 (2010) A69.
[14] H. Cheng, K. Scott, J. Power Sources 195 (2010) 1370.
[15] X. Li, Q. Huang, Z. Zou, B. Xia, H. Yang, Electrochim. Acta 53 (2008) 6662.
[16] M.H. Shao, T. Huang, P. Liu, J. Zhang, K. Sasaki, M.B. Vukmirovic, R.R. Adzic, Langmuir 22 (2006) 10409.
[17] W.E. Mustain, K. Kepler, J. Prakash, Electrochem. Commun. 8 (2006) 406.
[18] Y. Lin, X. Cui, X. Ye, Electrochem. Commun. 7 (2005) 267.
[19] J. Yang, J.J. Xu, Electrochem. Commun. 5 (2003) 306.
[20] R. Pattabiraman, Appl. Catal. A: Gen. 153 (1997) 9.
[21] C.C. Chang, T.C. Wen, H.J. Tien, Electrochim. Acta 42 (1997) 557.
[22] L.D. Burke, J.K. Casey, J. Electrochem. Soc. 140 (1993) 1284.
[23] G. Zheng, E.I. Altman, Surf. Sci. 462 (2000) 151 (and references therein).
[24] P.R. Van Rheenen, M.J. McKelvy, W.S. Glaunsinger, J. Solid State Chem. 67 (1987) 151.
[25] S. Ardizzone, G. Fregonara, S. Trasatti, Electrochim. Acta 35 (1990) 263.
[26] E.A. Sales, T.R.O. de Souza, R.C. Santos, H.M.C. Andrade, Catal. Today 107–108 (2005) 114.
[27] S.A. Jalal, D.-J. Zhang, M. Machida, Catal. Commun. 10 (2008) 192.
[28] V. Gomez-Serrano, F. Piriz-Almeida, C.J. Duran-Valle, J. Pastor-Villegas, Carbon 37 (1999) 1517.
[29] A.M. Vassallo, L.S.K. Pang, P.A. Cole-Clarke, M.A. Wilson, J. Am. Chem. Soc. 113 (1991) 7820.
[30] A. Fukunaga, S. Ueda, M. Nagumo, Carbon 37 (1999) 1081.
[31] N. Dementev, S. Osswald, Y. Gogotsi, E. Borguet, J. Mater. Chem. 19 (2009) 7904.
[32] W.P. Hoffman, US Patent 5271917, 1993;
    J.M. Skowronski, J. Therm. Anal. 16 (1979) 463.
[33] The International Centre for Diffraction Data®, http://www.icdd.com/ (the reference codes are 00-046-1043 for Pd and 00-041-1107 for PdO).
[34] O.S.G.P. Soares, J.J.M. Orfao, J. Ruiz-Martinez, J. Silvestre-Albero, A. Sepulveda-Escribano, M.F.R. Pereira, Chem. Eng. J. 165 (2010) 78.
[35] H. Cheng, W. Yuan, K. Scott, Electrochim. Acta 52 (2006) 466.
[36] J.S. Dong, T.-J. Park, S.-K. Ihm, Carbon 31 (1993) 427.
[37] N. Takami, A. Satoh, M. Hara, T. Ohsaki, J. Electrochem. Soc. 142 (1995) 371.
[38] R. Yazami, D. Guerard, J. Power Sources 43 (1993) 39.
[39] B. Simon, J.P. Boeure, M. Broussely, J. Power Sources 43 (1993) 65.
[40] J.O. Besenhard, M.W. Wagner, M. Winter, J. Power Sources 43 (1993) 413.
[41] S. Passerini, J.M. Rosolen, B. Scrosati, J. Power Sources 45 (1993) 333.
[42] J. Thevenin, R.H. Muller, J. Electrochem. Soc. 134 (1987) 237.
[43] N. Takami, T. Ohsaki, K. Inada, J. Electrochem. Soc. 139 (1992) 1849.
[44] R. Fong, U. von Sacken, J.R. Dahn, J. Electrochem. Soc. 137 (1990) 2009.
[45] M. Mirzaeian, P.J. Hall, J. Power Sources 195 (2010) 6817.
[46] F. Croce, F. Nobili, A. Deptula, W. Lada, R. Tossici, A. D'Epifanio, B. Scrosati, R. Marassi, Electrochem. Commun. 1 (1999) 605.
[47] J.Y. Song, H.H. Lee, Y.Y. Wang, C.C. Wan, J. Power Sources 111 (2002) 255.
[48] X. Yang, Y. Xia, J. Solid State Electrochem. 14 (2010) 109.
[49] J. Fan, P.S. Fedkiw, J. Power Sources 72 (1998) 165.
[50] T. Tonosaki, T. Oho, K. Isomura, K. Ogura, J. Electroanal. Chem. 520 (2002) 89.
[51] H. Arai, S. Muller, O. Haas, J. Electrochem. Soc. 147 (2000) 3584.
[52] H. Wang, H. Huang, S.L. Wunderz, J. Electrochem. Soc. 147 (2000) 2853.
[53] Z. Peng, S.A. Freunberger, L.J. Hardwick, Y. Chen, V. Giordani, F. Barde, P. Novak, D. Graham, J.-M. Tarascon, P.G. Bruce, Angew. Chem. Int. Ed. 50 (2011) 6351.
[54] J. Xiao, J. Hu, D. Wang, D. Hu, W. Xu, G.L. Graff, Z. Nie, J. Liu, J. Zhang, J. Power Sources 196 (2011) 5674.
[55] P. Poizot, S. Laruelle, S. Grugeon, L. Dupont, J.-M. Tarascon, Nature 407 (2000) 496.
[56] M.M. Thackeray, M.H. Rossouw, A. de Kock, A.P. de la Harpe, R.J. Gummow, K. Pearce, D.C. Liles, J. Power Sources 43–44 (1993) 289.
[57] L. Zhang, K. Lee, J. Zhang, Electrochim. Acta 52 (2007) 7964.
[58] D.R. Lide, CRC Handbook of Chemistry and Physics, 85th ed., CRC Press, New York, 2004.
[59] E. Rey, M.R. Kamal, R.B. Miles, B.S.H. Royce, J. Mater. Sci. 13 (1978) 812.
[60] D.B. Rogers, R.D. Shannon, J.L. Gillson, J. Solid State Chem. 3 (1971) 314.
[61] N. Jia, R.B. Martin, Z. Qi, M.C. Lefebvre, P.G. Pickup, Electrochim. Acta 46 (2001) 2863.
[62] S. Ahn, B.J. Tatarchuk, J. Electrochem. Soc. 142 (1995) 4169.
[63] P.B. Balbuena, Y. Wang, Lithium-Ion Batteries: Solid-Electrolyte Interphase, Imperial College Press, London, 2004 (chapter 1 and refs. cited).
[64] Y. Cheng, G. Wang, M. Yan, Z. Jiang, J. Solid State Electrochem. 11 (2007) 310.
[65] F. Mizuno, S. Nakanishi, Y. Lotani, S. Yokoishi, H. Iba, Electrochemistry 78 (2010) 403.
[66] S.A. Freunberger, Y. Chen, Z. Peng, J.M. Griffin, L.J. Hardwick, F. Barde, P. Novak, P.G. Bruce, J. Am. Chem. Soc. 133 (2011) 8040.
[67] B.D. McCloskey, D.S. Bethune, R.M. Shelby, G. Girishkumar, A.C. Luntz, J. Phys. Chem. Lett. 2 (2011) 1161.
[68] S.S. Zhang, D. Foster, J. Read, J. Power Sources 195 (2010) 1235.
[69] K. Reuter, C. Stampfl, M.V. Ganduglia-Pirovano, M. Scheffler, Chem. Phys. Lett. 352 (2002) 311.
[70] D.R. Rolison, P.L. Hagans, K.E. Swider, J.W. Long, Langmuir 15 (1999) 774.
[71] H. Conrad, G. Ertl, J. Kuppers, E.E. Latta, Surf. Sci. 65 (1977) 245.
[72] K. Ding, G. Yang, S. Wei, P. Mavinakuli, Z. Guo, Ind. Eng. Chem. Res. 49 (2010) 11415.
[73] J.J. Chen, E. Ruckenstein, J. Phys. Chem. 85 (1981) 1606.
[74] S. Specchia, P. Palmisano, E. Finocchio, M.A.L. Vargas, G. Busca, Appl. Catal. B: Environ. 92 (2009) 285.
[75] C.C. Chang, T.C. Wen, Mater. Chem. Phys. 47 (1997) 203.
[76] Y.-C. Wei, C.-W. Liu, H.-W. Lee, S.-R. Chung, S.-L. Lee, T.-S. Shan, J.-F. Lee, K.-W. Wang, Int. J. Hydrogen Energy 36 (2011) 3789.
[78] S. Mukerjee, S. Srinivasan, M.P. Soriaga, J. McBreen, J. Electrochem. Soc. 142 (1995) 1409.
[79] X. Ren, M.S. Wilson, S. Gottesfeld, J. Electrochem. Soc. 143 (1996) L12.
[80] L. Liu, C. Pu, R. Viswanathan, Q. Fan, R. Liu, E.S. Smotkin, Electrochim. Acta 43 (1998) 3657.
[81] H. Harker, C. Jackson, W.F.K. Wynne-Jones, Proc. R. Soc. Lond. Ser. A: Math. Phys. Sci. 262 (1961) 328.
[82] D.J.E. Ingram, J.G. Tapley, R. Jackson, R.L. Bond, A.R. Murnaghan, Nature 174 (1954) 797.